CHAPTER 49

Non-Oscillatory Spectral Element Chebyshev Method for Shock Wave Calculations

David Sidilkover*
George Em Karniadakis*

Abstract. A new algorithm based on spectral element discretization and non-oscillatory ideas is developed for the solution of hyperbolic partial differential equations. A conservative formulation is proposed based on cell averaging and reconstruction procedures, that employs a staggered grid of Gauss-Chebyshev and Gauss-Lobatto-Chebyshev discretizations. The non-oscillatory reconstruction procedure is based on ideas similar to those proposed by Cai et al in [2] but employs a modified technique which is more robust and simpler in terms of determining the location and strength of a discontinuity. It is demonstrated through model problems of linear advection, inviscid Burgers equation, and an one-dimensional Euler system that the proposed algorithm leads to stable, non-oscillatory spectrally accurate results away from discontinuities.

1. Introduction. Spectral element methods are high-order weighted residual techniques for the solution of partial differential equations typically encountered in fluid dynamics [9], [7]. Their success in the recent past in simulating complex flows derives from the flexibility of the method in representing accurately non-trivial geometries while preserving the good resolution properties of spectral methods [6]. In these simulations, however, both the geometry and the solution are described through smooth functions so that spectral element methods can obtain exponential accuracy by fully exploiting that regularity. There are numerous fluid dynamics applications however, where either very steep gradients or even jump-discontinuities are present e.g. interfaces in multiphase flows, flame fronts, or shocks in compressible flows. A straightforward application of high-order numerical methods in these situations is not possible, as large errors induced by the discontinuity (Gibbs phenomenon) propagate in the domain and eventually render the solution with oscillations everywhere.

One approach to succesfully simulating the aforementioned complex flows is to use

* Department of Mechanical and Aerospace Engineering and Program in Applied and Computational Mathematics, Princeton University, Princeton, NJ 08544

essentially non-oscillatory pseudospectral schemes developed for systems of hyperbolic partial differential equations

$$\mathbf{u}_t + \mathbf{f}(\mathbf{u})_x = 0 \tag{1.1}$$

(see [2] for the case of Fourier method). The main idea is to augment the spectral space by adding a non-smooth function, representing discontinuity. A conservative scheme can be obtained by defining cell averaged quantities in following the work of Cai et al. for Chebyshev methods [1]. A staggered grid of Gauss-Chebyshev and Gauss-Chebyshev-Lobatto collocation points is employed to accomodate the cell averages and point values. Point values are obtained from cell averages by using appropriate reconstruction procedure (possibly essentially non-oscillatory).

Although very accurate, the non-oscillatory spectral methods described in these previous works are limited to computational domains with highly regular nodal point distribution (and also periodic for Fourier method). In the current, work we attempt to relax these constraints by substituting for the higher-order scheme a spectral element method [9], [7]. In the spectral element discretization the computational domain is broken into several subdomains (macro-elements) whithin which data and unknowns are represented as spectral expansions in terms of general eigenfunctions - solutions of the singular Sturm-Liuville problems, i.e. Chebyshev polynomials, Legendre polynomials, etc. The discrete equations are derived via variational statements, so that the unknowns at each node represent values of the unknown field variable. This approach and its variants [6],[11],[8] results in exponential (spectral-like) converegnce for infinitely smooth solutions.

The main idea presented in this work is to modify the Chebyshev Lagrangian interpolant basis of the spectral element formulation by adding a non-smooth function, representing discontinuity. A new robust and efficient technique is also proposed for estimating the discontinuity location and strength. As a result the proposed non-oscillatory reconstruction procedure implemented on a staggered Chebyshev spectral element grid leads to stable solutions free of oscillations. The incorporation of a high-order filter [14] results in recovering spectral-like accuracy away from discontinuity.

The paper is organized as follows: In Section 2, we introduce the basic ideas upon which our conservative spectral element formulation is based (cell averaging and reconstruction procedures). In Section 3, the non-oscillatory cell averaging and reconstruction are presented. In Section 4, we describe model problems used in this work together with some additional aspects of reconstruction (interfacial constraint). In Section 5, we describe the entire algorithm and briefly review its components (time-marching scheme, filter, flux limiter). Finally the results are presented in Section 6, followed by a brief discussion in Section 7.

2. Cell averages and reconstruction: smooth function.

2.1. Cell averages. In the general case that we consider in this work the nodal points are distributed in a non-uniform manner and thus we need to define appropriate cell averaged quantities. In particular, adopting the terminology explained in Fig.2.1

the cell averaged velocity $\bar{u}_j$ is given by,

$$\bar{u}_j \equiv \bar{u}(x_j,t) = \frac{1}{x_{i^+} - x_{i^-}} \int_{x_{i^-}}^{x_{i^+}} u(x,t)dx \tag{2.1}$$

Given this definition, equation (1) can be integrated along a cell extending from i^- to i^+ as follows,

$$\frac{d\bar{u}_j}{dt} + \frac{f(u_{i^+}) - f(u_{i^-})}{\Delta x_j} = 0 \tag{2.2}$$

where we have also defined

$$\Delta x_j \equiv x_{i^+} - x_{i^-}. \tag{2.3}$$

The above equation therefore suggests that the fluxes $f(u)$ should be evaluated at the ends of the cell using *de-averaged* (reconstructed) velocity values; this formulation leads to the conservative (or flux) form of the semi-discrete wave equation.
In the following, we define cell averaged quantities for two particular discretizations: first, spectral (Chebyshev) discretizations; and second, spectral element (Chebyshev) discretizations. Proceeding with the first case we refer to Fig.2.1 where the set of points j at which cell averaged quantities are defined are simply the midpoints of the cell.
A spectral-Chebyshev expansion corresponds to a non-uniform distribution of points with cells of variable size Δx_j. Following the formulation of Cai et al [1] we select the set of points j to be the Gauss-Chebyshev points (see Fig.2.2) defined by,

$$x_j = \cos((j-1/2)\Delta\theta) \quad \text{where} \quad \Delta\theta = \pi/N \quad \text{and} \quad 1 \le j \le N \tag{2.4}$$

while the end points i^+, i^- of each cell are the Gauss-Lobatto points defined as

$$x_i = \cos(i\Delta\theta) \quad 0 \le i \le N. \tag{2.5}$$

Using these two sets of points and the definition (2.1) a Chebyshev spectral expansion then of the form,

$$u(x) = \sum_{k=0}^{N} a_k T_k(x) \tag{2.6}$$

after averaging becomes,

$$\bar{u}(x) = \sum_{k=0}^{N} a_k \, \bar{T}_k(x) \tag{2.7}$$

where the cell averaged Chebyshev polynomial is given by,

$$\bar{T}_0 = 1 \tag{2.8}$$

$$\bar{T}_1 = \frac{1}{2}\sigma_1 U_1(x) \tag{2.9}$$

$$\bar{T}_k = \frac{1}{2}[\sigma_k U_k(x) - \sigma_{k-2} U_{k-2}(x)] \quad \forall k \ge 2 \tag{2.10}$$

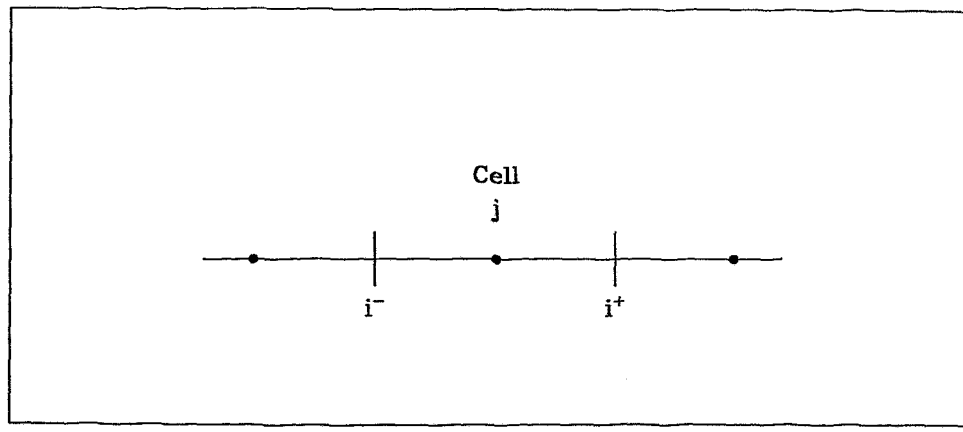

FIG. 2.1. *Cell average and point values.*

where

$$\sigma_k = \frac{\sin(k+1)\frac{\Delta\theta}{2}}{(k+1)\sin(\frac{\Delta\theta}{2})}. \tag{2.11}$$

Here we have introduced $U_k(x) = \frac{1}{k+1}T'_{k+1}(x)$ to be the second kind of the Chebyshev polynomials.

In the spectral element discretization the domain is broken up into several macro-elements (Fig.2.3) within which the velocity is expanded in terms of Chebyshev polynomials; C^0 continuity is imposed at the elemental boundaries.

Here, we establish the connection between the local (elemental) reference system and the global (physical) coordinate system. For the set of Gauss-Lobatto-Chebyshev points their local coordinate in the k-th element is given by,

$$r_i^k = -\cos(\frac{\pi i}{N}) \quad 0 \le i \le N \tag{2.12}$$

which are related to the global coordinate x through the equation

$$x = \frac{L^k}{2}r^k + \frac{x_L^k + x_R^k}{2}; \tag{2.13}$$

here x_L^k and x_R^k denote the left and right coordinate of the elemental boundaries.

The interpolant of $u(x)$ in the k-th element is then represented as,

$$u^k(r) = \sum_{i=0}^{N} h_i(r^k)u_i^k. \tag{2.14}$$

Here, u_i^k are nodal values of u, and h_i are shape functions corresponding to element k and node i, with property $h_i(r_j^k) = \delta_{ij}$ is the Kronecker-delta symbol. Expressions for

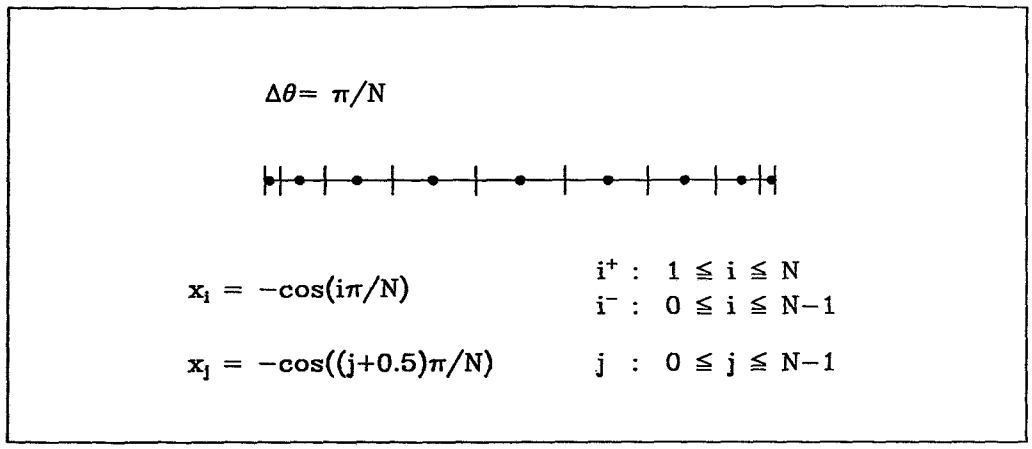

FIG. 2.2. *Spectral Chebyshev method. The set of points j defines the cell averaged quantities, while the point values i are used in evaluating the fluxes.*

these Lagrangian interpolants (as well as for their derivatives) in terms of Chebyshev or Legendre polynomials can be found in [5].

Therefore, in the k-th element an expansion of the form

$$u^k(x) = \sum_{i=0}^{N} u_i^k h_i(x) \tag{2.15}$$

defined on the Gauss-Lobatto-Chebyshev points after the application of the averaging operator takes the form

$$\bar{u}^k(x) = \sum_{i=0}^{N} u_i^k \bar{h}_i(x) \tag{2.16}$$

where u_i^k are the point values for element k and x refers to the local coordinate; $h_i(x)$ and $\bar{h}_i(x)$ are the Gauss-Lobatto-Chebyshev-Lagrangian interpolant and its corresponding cell averaged function obtained from,

$$h_i(x) = \frac{2}{N} \sum_{p=0}^{N} \frac{1}{\bar{c}_i \bar{c}_p} T_p(x_i) T_p(x) \quad 0 \le i \le N \tag{2.17}$$

$$\bar{h}_i(x) = \frac{2}{N} \sum_{p=0}^{N} \frac{1}{\bar{c}_i \bar{c}_p} T_p(x_i) \bar{T}_p(x) \quad 0 \le i \le N \tag{2.18}$$

where $c_n = 1$ if $n \neq 0, N$ and $c_n = 2$ otherwise. In matrix form the above cell averaging procedure can be written as,

$$\bar{u}_j{}^k = \mathbf{A}_{ji}^k \mathbf{u}_i^k \quad 0 \le i \le N \quad 0 \le j \le N \tag{2.19}$$

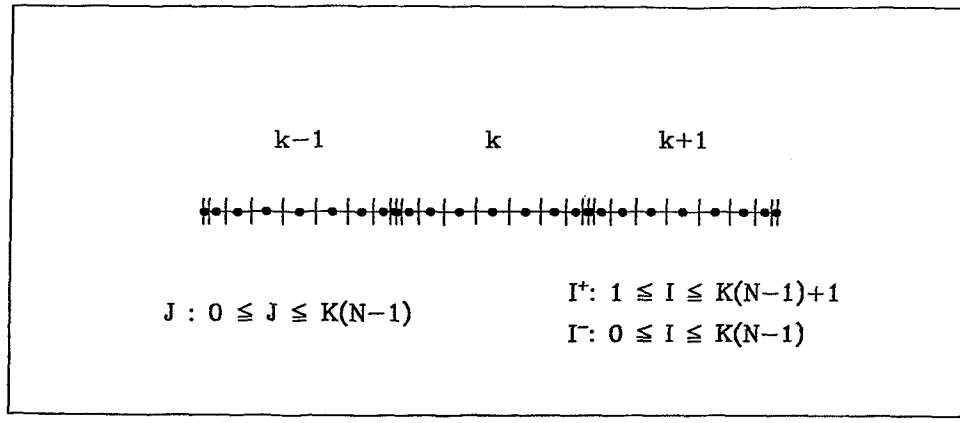

FIG. 2.3. *Spectral element Chebyshev discretization. J's are used for global indexing of cell averaged quantities and I's - for global indexing of point values.*

where the cell averaging matrix is defined as $A^k_{ji} = \bar{h}_i(x_j)$; here x_j refers to local coordinate. Based on the nodal cell averaged values obtained from (2.19) the corresponding polynomial can be constructed using Lagrangian interpolation, i.e.

$$\bar{u}(x) = \sum_{j=1}^{N} \bar{u}_j{}^k g_j(x) \tag{2.20}$$

where the Gauss-Chebyshev-Lagrangian interpolant is given by,

$$g_j(x) = (-1)^{j+1} \frac{1-x_j^2}{x-x_j} \frac{T_N(x)}{N} \quad 1 \le j \le N \tag{2.21}$$

Having constructed a cell averaging procedure for the spectral element discretization we proceed next with the inverse operation of de-averaging and recovering point values for the evaluation of fluxes in equation (2.2).

2.2. Reconstruction and point values. The reconstruction operation can also be put into matrix form. We consider first the polynomial describing the cell averaged values,

$$\bar{u}(x) = \sum_{j=1}^{N} \bar{u}^k_j g_j(x). \tag{2.22}$$

An alternative to (2.21) expression for the Gauss-Chebyshev-Lagrangian interpolant is the following,

$$g_j(x) = \sum_{p=0}^{N-1} \frac{2}{N\bar{c}_p} T_p(x_j) T_p(x). \tag{2.23}$$

We can also express the $g_j(x)$ in terms of the second kind Chebyshev polynomials; to this end we recall that,

$$T_p(x) = \frac{1}{2}[U_p(x) - U_{p-2}(x)] \quad \forall p \geq 2. \tag{2.24}$$

Using the above equation we can rewrite $g_j(x)$ as follows,

$$g_j(x) = \sum_{p=0}^{N-1} \lambda_p^j \sigma_p U_p(x) \quad 1 \leq j \leq N. \tag{2.25}$$

Here we have defined:

$$\lambda_p^j = \frac{1}{N} T_p(x_j) \quad \text{for} \quad p = N-2, N-1 \tag{2.26}$$

$$\lambda_p^j = \frac{1}{N}[T_p(x_j) - T_{p+2}(x_j)] \quad \text{for} \quad 0 \leq p \leq N-3. \tag{2.27}$$

The interpolating polynomial corresponding to point values (Gauss-Chebyshev-Lobatto points) can then constructed using the *de-averaged* Lagrangian interpolants G_j as follows,

$$u(x) = \sum_{j=1}^{N} \bar{u}_j^k G_j(x). \tag{2.28}$$

The cell averaged second kind Chebysev polynomial is obtained using the definition of equation (2.1) (see details in [1]):

$$\bar{U}_p(x) = \sigma_p U_p(x) \tag{2.29}$$

with σ_p obtained from equation (2.11). To determine $G_j(x)$ therefore we consider (2.28-2.29) and (2.22-2.25) and thus we obtain,

$$G_j(x) = \sum_{p=0}^{N-1} \frac{\lambda_p^j}{\sigma_p} U_p(x). \tag{2.30}$$

To recover the point values u_i we simply set $x = x_i$ in the interpolating polynomial $u(x)$. In matrix form the reconstruction procedure (on elemental level) can be written in the form,

$$\mathbf{u_i} = \mathbf{g_{ij}^* \bar{u}_j} \quad \text{for} \quad 1 \leq j \leq N; \quad 1 \leq i \leq N \tag{2.31}$$

where

$$g_{ij}^* = G_j(x_i). \tag{2.32}$$

Based on these N point values the interpolating polynomial $u(x)$ can then be constructed from equation (2.28). This local reconstruction procedure is then repeated for all elements. To form a global interpolating polynomial however we need to impose a continuity condition at elemental interfaces as we explain in the next Section.

2.3. Interfacial constraint. The interpolation polynomial $u(x)$ constructed based on the Gauss-Lobatto-Chebyshev points is of degree N while the polynomial we obtain from the reconstruction procedure is of degree $(N-1)$. The additional information needed to uniquely define $u(x)$ comes from requiring continuity of the solution at the interfacial nodal points. For the k-th element for example we require that its rightmost nodal value and the leftmost nodal value of element $(k+1)$ will be equal (say, to some value u_γ). This can be accomplished for $(k+1)$-th element by adding an extra term to the $(N-1)$-th order polynomial, as follows

$$u^{k+1}(r) = \sum_{j=1}^{N} \bar{u}_j^{k+1} G_j(r) + (1-r) T_N'(r) \frac{\delta u^k}{2N^2}, \tag{2.33}$$

where δu^k can be defined by

$$\delta u^k = u_\gamma - \sum_{j=1}^{N} \bar{u}_j^{k+1} G_j(-1). \tag{2.34}$$

Here the coordinate $r \in (-1,1)$ refers to the local element coordinate (see Sec.2.1).

Note that the expression $(1-r)T_N'(r)$ attains zero values at all the Gauss-Lobatto-Chebyshev points of the $(k+1)$-th element except the leftmost one. Therefore, implementing (2.33),(2.34) is equivalent in practice to requiring only the leftmost point value to be equal to u_γ. The rest of the point values of the $(k+1)$-th element remain unchanged. The same will be true for the k-th element and its rightmost point value.

The only undetermined quantity is u_γ. The value of u_γ should be set either to $\sum_{j=1}^{N} \bar{u}_j^{k+1} G_j(-1)$ or to $\sum_{j=1}^{N} \bar{u}_j^{k} G_j(1)$ depending on the direction (i.e. sign of the advection velocity) of the problem. We will elaborate on this point in Section 4.

3. Cell averages and reconstruction: discontinuous function. The main difficulty in applying spectral methods to discontinuous problems is the Gibbs phenomenon. If a discontinuous function is approximated by a spectral expansion (Chebyshev, Fourier etc.), the approximation is only $O(1/N)$ accurate in smooth regions and contains $O(1)$ oscillations near the discontinuity. When spectral methods are applied to partial differential equations with discontinuous solutions, the Gibbs phenomenon may also lead to numerical instability.

An interesting approach to construct a non-oscillatory spectral approximation to a discontinuous function has been recently proposed in [2]. Let $u(x)$ be a piecewise C^∞ function with a jump discontinuity at point x_s and with a jump $[u]_{x_s}$. The key idea in [2] was to augment the Fourier spectral space with a saw-tooth function. It was shown that the approximation using the augmented spectral space will be non-oscillatory if the saw-tooth function approximates the magnitude and the location of the discontinuity with second order accuracy. In addition, a method for estimating the discontinuity parameters with specified accuracy based on the spectral expansion coefficients was suggested. More recently, it was pointed in [3] that a first order accurate approximation of discontinuity magnitude also leads to non-oscillatory behavior.

Numerical experiments with discontinuous solutions using the Chebyshev spectral space augmented by a step function and cell averaging approach were reported in [1].

Here we extend this approach to the context of the spectral elements. In addition, we present a very simple and reliable method which allows the estimation of the discontinuity parameters with an accuracy required for obtaining a non-oscillatory approximation.

In this Section we denote for simplicity the entire array of cell averages defined at the Gauss-Chebyshev points (see Fig.2.3) (regardless of which element they belong to) by $\bar{u}_J$

$$\bar{u}_J, \text{ for } 1 \leq J \leq K \cdot (N-1),$$

where K is the number of spectral elements covering the domain and N the number of Gauss-Lobatto-Chebyshev points in each element. We also denote by u_I the entire array of point values defined at the Gauss-Lobatto-Chebyshev points (as shown in Fig.2.3), i.e.

$$u_I, \text{ for } 0 \leq I \leq K \cdot (N-1)+1.$$

3.1. Reconstruction of point values. We assume that the cell-averaged values of a discontinuous function $\bar{u}_J$ are given. Here we propose a new reconstruction algorithm based on a simple and reliable procedure for estimating the discontinuity parameters with specified accuracy. The main steps of the algorithm are as follows:

Algorithm R:

- Step 1: Find a cell J_s such that,

$$|\bar{u}_{J_s+1} - \bar{u}_{J_s-1}| = \max_{2 \leq J \leq K\cdot(N-1)-1} |\bar{u}_{J+1} - \bar{u}_{J-1}|$$

- Step 2: Determine the discontinuous component,

$$\bar{u}^d_J = \begin{cases} \bar{u}_{J_s-1}, & \text{if } 1 \leq J \leq J_s - 1 \\ \bar{u}_{J_s}, & \text{if } J = J_s \\ \bar{u}_{J_s+1}, & \text{if } J_s + 1 \leq J \leq K \cdot (N-1) \end{cases}$$

- Step 3: Determine the continuous component,

$$\bar{u}^c_J = \bar{u}_J - \bar{u}^d_J, \text{ for } 1 \leq J \leq K \cdot (N-1)$$

- Step 4: Find I^-_s, I^+_s such that J_s denotes the cell corresponding to the interval $[x_{I^-_s}, x_{I^+_s}]$.

$$u^d_I = \begin{cases} \bar{u}_{J_s-1}, & \text{if } 1 \leq I \leq I^-_s \\ \bar{u}_{J_s+1}, & \text{if } I^+_s \leq I \leq K \cdot (N-1)+1 \end{cases}$$

- Step 5: Obtain point values u^c_I from $\bar{u}^c_m$ using the procedure presented in Section 2 (equation (2.28)).
- Step 6: Obtain

$$u_I = u^c_I + u^d_I \text{ for } 1 \leq I \leq K \cdot (N-1)+1$$

It is obvious that the pair of cell averages $\bar{u}_{J_s-1}$ and $\bar{u}_{J_s+1}$ represents the discontinuity magnitude with first order accuracy. It has been shown in [12] however that three cell averaged values $\bar{u}_{J_s-1}$, $\bar{u}_{J_s}$ and $\bar{u}_{J_s+1}$ contain information about the discontinuity location up to second order accuracy. However, our algorithm does not require explicit information about the discontinuity location. As a result, we obtain a very simple and reliable algorithm for non-oscillatory reconstruction. The current algorithm is based entirely on the cell averaged values in the physical space and not on the coefficients of a spectral expansion. Therefore, it fits naturally into the context of the spectral element method as well as into the context of spectral methods.

3.2. Cell averages. As in the smooth case we assume that the point values of a function are known and that the function contains a single jump discontinuity at the point x_s. Again, we decompose a given discrete function into two parts: discontinuous and smooth, the smooth part can be averaged using the procedure described in Section 2, The cell averages corresponding to the discontinuous part can be computed directly using the following algorithm:

Algorithm A:

- Step 1: Find point values I_s^+, I_s^- such that

$$x_{I_s^-} \le x_s \le x_{I_s^+}.$$

- Step 2: Evaluate the discontinuous component

$$u_I^d = \begin{cases} u_{I_s^-}, & \text{if } 1 \le I \le I_s^- \\ u_{I_s^+}, & \text{if } I_s^+ \le I \le K \cdot (N-1) + 1 \end{cases}$$

- Step 3: Obtain the continuous component

$$u_I^c = u_I - u_I^d, \text{ for } 1 \le I \le K \cdot (N-1) + 1$$

- Step 4: For the cell corresponding to the interval $[x_{I_s}, x_{I_s} + 1]$, defined by J_s, determine

$$\bar{u}_J^d = \begin{cases} u_{I_s^-}, & \text{if } 1 \le J < J_s \\ \frac{u_{I_s^-}(x_s - x_{I_s^-}) + u_{I_s^+}(x_{I_s^+} - x_s)}{x_{I_s^+} - x_{I_s^-}}, & \text{if } J = J_s \\ u_{I_s^+}, & \text{if } J_s < J \le K \cdot (N-1) \end{cases}$$

- Step 5: Evaluate $\bar{u}_J^c$ for $1 \le J \le K \cdot (N-1)$ applying the averaging procedure to u_I^c $(1 \le I \le K \cdot (N-1) + 1)$.
- Step 6: Define $\bar{u}_J = \bar{u}_J^c + \bar{u}_J^d$ for $1 \le I \le K \cdot (N-1) + 1$.

4. Hyperbolic equations. The numerical results reported in this paper use three standard examples: first linear advection problem and the inviscid Burgers equation and then one-dimensional Euler equations of gas dynamics.

4.1. Linear advection. The model problem we consider is the initial value problem given by

$$\begin{cases} u_t + a u_x = 0, \\ u(x,0) = \phi(x), \\ u(0,t) = \psi(t), \end{cases} \tag{4.1}$$

where $\phi(x)$ and $\psi(t)$ are given functions and a is a constant representing the advection velocity.

The interfacial condition is imposed according to the sign (direction) of the advection speed, as follows

$$u_\gamma = \begin{cases} u_0^{k+1}, & \text{if } a < 0, \\ u_N^k, & \text{if } a \geq 0, \end{cases} \tag{4.2}$$

4.2. Inviscid Burgers equation. The model problem we consider is the initial value problem for the inviscid Burgers equation,

$$\begin{cases} u_t + (\frac{u^2}{2})_x = 0, \\ u(x,0) = \phi(x), \\ u(0,t) = \psi(t). \end{cases} \tag{4.3}$$

Note, that the Burgers equation can be rewritten in quasilinear form as follows

$$u_t + u u_x = 0. \tag{4.4}$$

It is clear from (4.4) that u plays the role of the advection velocity in this case.

To impose the interfacial continuity constraint we determine the direction according to the Roe-speed (see [10])

$$\tilde{a} = \frac{u_N^{k-1} + u_0^k}{2}, \tag{4.5}$$

and thus

$$u_\gamma = \begin{cases} u_0^{k+1}, & \text{if } \tilde{a} < 0, \\ u_N^k, & \text{if } \tilde{a} \geq 0. \end{cases} \tag{4.6}$$

4.3. One-dimensional Euler equations of gas dynamics. The system of Euler equations for polytropic gas in one dimension is given by:

$$\mathbf{u}_t + \mathbf{f}(\mathbf{u})_x = 0, \tag{4.7}$$

whith

$$\mathbf{u} = \begin{pmatrix} \rho \\ m \\ E \end{pmatrix}, \quad \mathbf{f} = \begin{pmatrix} \rho q \\ qm + P \\ q(P+E) \end{pmatrix}, \tag{4.8}$$

$$P = (\gamma - 1)(E - \frac{1}{2}\rho q^2), \tag{4.9}$$

where ρ denotes density, q is velocity, P pressure, E total energy, $m = \rho q$ is the momentum and γ is the ratio of the specific heats of a polytropic gas.

While the discretization of the Euler system using the cell-averaging approach is straightforward, the imposition of the interfacial condition requires further discussion.

Interfacial condition

Consider the Jacobian matrix of the system given by $A(\mathbf{u}) = \partial \mathbf{f}/\partial \mathbf{u}$.

The right-eigenvectors of A are

$$\mathbf{r}_1(\mathbf{u}) = \begin{pmatrix} 1 \\ q - c \\ H - qc \end{pmatrix}, \quad \mathbf{r}_2(\mathbf{u}) = \begin{pmatrix} 1 \\ q \\ \frac{1}{2}q^2 \end{pmatrix}, \quad \mathbf{r}_3(\mathbf{u}) = \begin{pmatrix} 1 \\ q + c \\ H + qc \end{pmatrix}, \tag{4.10}$$

where $c = \sqrt{\gamma P/\rho}$ is the speed of sound and H represents enthalpy and is defined by

$$H = \frac{(E + P)}{\rho} = \frac{c^2}{\gamma - 1} + \frac{1}{2}q^2. \tag{4.11}$$

The left-eigenvectors of A are

$$\begin{array}{lll} \mathbf{l}_1(\mathbf{u}) = \frac{1}{2c^2}(& (2c + q(\gamma-1))\frac{q}{2}, & -c - q(\gamma-1), \quad \gamma - 1), \\ \mathbf{l}_2(\mathbf{u}) = \frac{1}{c^2}(& c^2 - (\gamma-1)\frac{q^2}{2}, & (\gamma-1)q, \quad -(\gamma-1)), \\ \mathbf{l}_3(\mathbf{u}) = \frac{1}{2c^2}(& -(2c - q(\gamma-1))\frac{q}{2}, & c - q(\gamma-1), \quad \gamma - 1). \end{array} \tag{4.12}$$

Let us denote the matrix of right-eigenvectors of the Jacobian $A = A(\tilde{\mathbf{u}})$ as,

$$R = (\mathbf{r}_1(\tilde{\mathbf{u}}), \mathbf{r}_2(\tilde{\mathbf{u}}), \mathbf{r}_3(\tilde{\mathbf{u}})) \tag{4.13}$$

and the matrix of left eigenvectors as,

$$L = \begin{pmatrix} \mathbf{l}_1(\tilde{\mathbf{u}}) \\ \mathbf{l}_2(\tilde{\mathbf{u}}) \\ \mathbf{l}_3(\tilde{\mathbf{u}}) \end{pmatrix}, \tag{4.14}$$

where $\tilde{\mathbf{u}}$ is Roe-averaged state between the states $\mathbf{u}_N^k$ and $\mathbf{u}_0^{k+1}$ (see [10]).

Then

$$L \cdot A \cdot R = \begin{pmatrix} \lambda_1 & 0 & 0 \\ 0 & \lambda_2 & 0 \\ 0 & 0 & \lambda_3 \end{pmatrix}, \tag{4.15}$$

where the eigenvalues of A are given by

$$\lambda_1 = q - c, \quad \lambda_2 = q, \quad \lambda_3 = q + c. \tag{4.16}$$

The characteristic variables $\mathbf{v} = L \cdot \mathbf{u}$ can be introduced for both states as

$$\begin{array}{ll} \mathbf{v}_0^{k+1} & = L \cdot \mathbf{u}_0^{k+1} \\ \mathbf{v}_N^k & = L \cdot \mathbf{u}_N^k. \end{array} \tag{4.17}$$

Then the values to be imposed at the interface can be defined by

$$(\mathbf{v}_\gamma)_i = \begin{cases} (\mathbf{v}_0^{k+1})_i, & \text{if } \lambda_i < 0, \\ (\mathbf{v}_N^k)_i, & \text{if } \lambda_i \geq 0, \end{cases} \qquad i = 1,2,3, \tag{4.18}$$

and can be transformed back to the physical variables by

$$\mathbf{u}_\gamma = R \cdot \mathbf{v}_\gamma \tag{4.19}$$

A similar procedure can be used to impose Dirichlet boundary conditions.

5. Algorithm. In this section we describe in some detail the time-stepping procedure, filtering, and flux-limiting which are used in the overall algorithm.

5.1. Time discretization. An explicit time-stepping scheme is used which corresponds to the Adams-Bashforth scheme of order $M = 1$ (Euler), order $M = 2$ or 3 in the form,

$$\bar{u}_J^{n+1} = \bar{u}_J^n - \frac{\Delta t}{\Delta x_J} \sum_{q=0}^{M} \beta_q [f_{I+} - f_{I-}]^{n-q}, \tag{5.1}$$

where β_q are appropriate weight coefficients [4]. The higher-order fluxes f_I are computed at the Gauss-Lobatto-Chebyshev points after point values have been reconstructed from the cell averaged field $\bar{u}_J$.

5.2. Filter. In our experiments we used the filter developed recently by Vandeven [14]. It is given by

$$\sigma_p(x) = 1 - \frac{(2p-1)!}{(p-1)!^2} \int_0^x [t(1-t)]^{p-1} dt, \tag{5.2}$$

where p is the order of the filter. It has been shown in [14] that a p-th order accuracy can be recovered away from discontinuity.

5.3. Flux limiter. Here we describe a flux limiter used in our experiments. Let us denote by

$$\begin{aligned} \delta^L &= u_I - \bar{u}_J \\ \delta^R &= u_I - \bar{u}_{J+1} \end{aligned}$$

and

$$\begin{aligned} a_0 &= \bar{u}_{J+1} - \bar{u}_J \\ a_{-1} &= \bar{u}_J - \bar{u}_{J-1} \\ a_1 &= \bar{u}_{J+2} - \bar{u}_{J+1}. \end{aligned}$$

Then we define

$$\begin{aligned} \Psi_1^L &= \max(0, \min(1, \tfrac{a_0}{\delta^L})) \\ \Psi_2^L &= \max(0, \min(1, \tfrac{a_{-1}}{\delta^L})) \\ \Psi^L &= \min(\Psi_1^L, \Psi_2^L), \end{aligned} \tag{5.3}$$

and evaluate,

$$u_I^L = \bar{u}_J + \Psi^L \cdot \delta^L. \tag{5.4}$$

Following a similar procedure we define

$$\begin{aligned} \Psi_1^R &= \max(0, \min(1, \tfrac{a_0}{\delta^R})) \\ \Psi_2^R &= \max(0, \min(1, \tfrac{a_1}{\delta^R})), \\ \Psi^R &= \min(\Psi_1^R, \Psi_2^R), \end{aligned} \tag{5.5}$$

and evaluate

$$u_I^R = \bar{u}_{J+1} + \Psi^R \cdot \delta^R. \tag{5.6}$$

Finally the flux is computed according to

$$f_I = \frac{1}{2}[(f(u_I^R) + f(u_I^L)) - |\tilde{a}_I|(u_I^R - u_I^L)] \tag{5.7}$$

where $\tilde{a}_I$ is Roe-averaged state between u_I^R and u_I^L. Notice the apparent similarity of this limiter to Roe non-compressive limiter (see [13]).

5.4. Description of the algorithm.

- Step 1: Employ **Algorithm A** to evaluate field of cell averages $\bar{u}_J(0)$ on the Gauss-Chebyshev mesh corresponding to the initial condition $u(x, 0)$.
- Step 2: Compute the transportive fluxes f_I at each Gauss-Lobatto-Chebyshev point.
- Step 3: Advance (explicitly) the cell averages from the previous time level n to obtain $\bar{u}_J^{n+1}$.
- Step 4: Reconstruct point values u_I from the cell averages employing **Algorithm R.**
- Step 5: If the target time is not achieved go to Step 2.

6. Numerical results. In this section we will report several numerical experiments with the developed algorithm, including approximation results, linear advection, inviscid Burgers equation and the 1-D Euler system analyzed in Section 4

Non-oscillatory averaging and reconstruction.

Our first experiment reported here concerns a static non-oscillatory averaging followed by reconstruction. Given are the point values of the following function

$$u = \frac{4}{1 + \cos^2 y} - 3, \text{ where } y = \begin{cases} \frac{\pi}{40}(x - 7), & \text{if } 0 \le x \le 5, \\ \frac{\pi}{40}(x - 9), & \text{if } 5 < x \le 10. \end{cases} \tag{6.1}$$

This function has a jump discontinuity at $x_s = 5$. First, we evaluate cell averages of a given discrete function using **Algorithm A**, and then, we reconstruct the point values from the cell averages using **Algorithm R.** In Fig.6.1 we plot on the logarithmic scale the errors corresponding to three different discretizations. In each case the discretization consists of 5 spectral elements ($K = 5$), whith each element containing $N = 20, 40, 80$ points. The Vandeven filter of orders $p = 5, 10, 20$ was applied for

each case respectively to the Chebyshev spectrum of the smooth component on each element both in averaging and reconstruction procedure. This filtering was essential in order to obtain an exponential accuracy shown in the Fig.6.1 away from discontinuity.

Linear advection of discontinuous solution.

Consider the initial boundary value problem for the linear advection problem (4.1) for $x \in [0, 10]$, $a = 1$ and

$$\phi = \begin{cases} .5, \text{ for } x \leq 5, \\ 1.5, \text{ for } x > 5, \end{cases}$$

In Fig.6.2 we plot the numerical solution for $N = 64$, $K = 1$ (global spectral method) at time $t = 2.0$. In Fig.6.3 we plot the numerical solution to problem (4.1) with initial conditions given by (6.1) for $N = 40$, $K = 5$ at time $t = 1.0$. For both cases exponential convergence is obtained away from discontinuity.

Inviscid Burgers equation.

We consider the initial value problem in the interval $x \in [0, 6]$ with initial conditions given by

$$u(x, 0) = 0.3 + 0.7 \sin \frac{\pi x}{3}.$$

This initially smooth problem develops eventually a shock discontinuity in the solution. The exact solution is easily obtained, and is used the accuracy of of the proposed algorithm.

In Fig.6.4 we plot for $N = 20$, $K = 8$ at time $t = 2.0$. The pointwise errors are plotted on the logarithmic scale on Fig.6.5 for $K = 8$, and $N = 5, 10, 20$. The Vandeven filter of orders 4, 8 and 16 respectively was used. In all these experiments the non-oscillatory reconstruction was performed after the estimated discontinuity magnitude became larger than 0.4. (We observed that the results are not very sensitive to the particular value of the threshold.) Also, the limiter described in Sec.5.3 was employed here in the interval of 10 gridpoints around the cell containing discontinuity (except at points next to that cell - one on each side). Forward Euler time stepping was used at these points to advance cell averages. We found in our experiments with this example, that applying the global Chebyshev spectral method with non-oscillatory reconstruction and filtering the spectrum of the smooth part resulted in a very poor accuracy ($O(1)$ error) in the large part of the domain. This seems to be related to the creation of shock in this case. Large differences occur between several cell averaged values at that time. However, the non-oscillatory reconstruction method treats only 3 subsequent cells. Applying flux limiters in this part of the domain restores algebraic convergence there. Employing spectral elements led to localizing of this region within one element, as we observe on Fig.6.4.

One-dimensional Euler gas dynamics equations.

Here we present our numerical experiments with the test problem considered in [1, 3]. We consider the following initial condition for (4.7),

$$(6.2) \quad \begin{cases} \rho_l = 3.857143, \ q_l = 2.629367, \ P_l = 10.33333 & -5 \leq x \leq -4, \\ \rho_r = 1 + \varepsilon \sin \pi x, \ q_r = 0, \ P_r = 1 & -4 < x \leq 5, \end{cases}$$

where $\varepsilon = 0.2$. The solution to (6.2) models the interaction between a moving shock and sinusoidal density disturbances (see [1, 3]). In Fig.6.6 we display the density profile for $N = 10$ and $K = 22$ (corresponding to 201 grid points) at time $t = 1.8$. The discontinuity cell was located using the momentum equation. For comparison reason we also plot the solution obtained by the second order MUSCL scheme with $N = 200$ in Fig.6.6.

7. Discussion. In this work we have formulated an algorithm based on spectral element discretization and essentially non-oscillatory approximations concepts. The results show that this approach leads to a stable method, capable of producing exponentially accurate solutions away from discontinuities. There is also indication that blending the non-oscillatory reconstruction ideas and flux limiters may lead to a significant improvement in the quality of the results. The conclusion can be formulated as follows: inspite of the rough numerical treatment in the neighborhood close to discontinuity the accuracy away of discontinuity does not deteriorate. Moreover, the method is capable of resolving very accurately fine structures arising due to interactions of the shock with disturbances.

The generalization of the present method for the case of multiple discontinuities is straightforward. However, it seems that the method in its current form is not capable of treating rarefaction waves.

Acknowledgements. We would like to thank Professor David Gottlieb for many helpful suggestions. We would also like to thank John Giannakouros and Anne Bourlioux for many stimulating discussions. This work wa supported by AFOSR Grant number 90-0261 and by ONR Grant number N00014-82-C-0451.

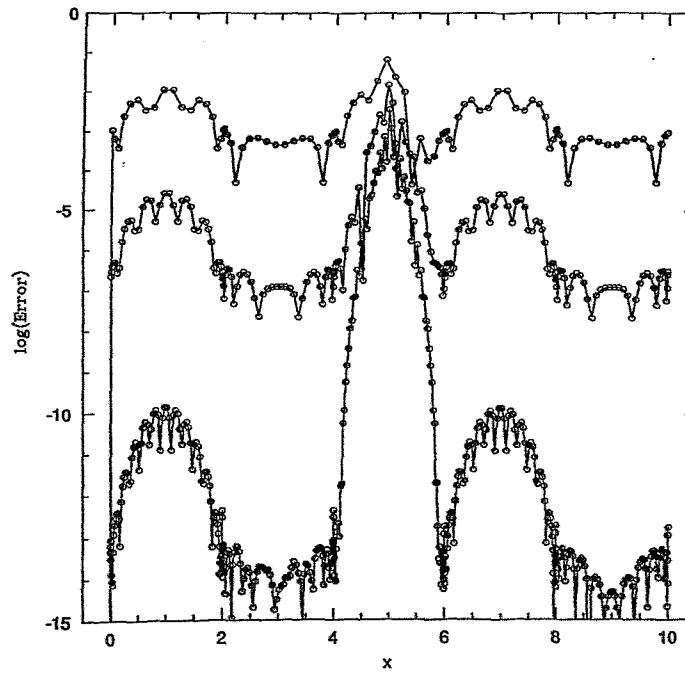

FIG. 6.1. *Averaging and reconstruction of a discontinuous function. Errors on the logarithmic scale,* $N = 5$, $K = 20, 40, 80$.

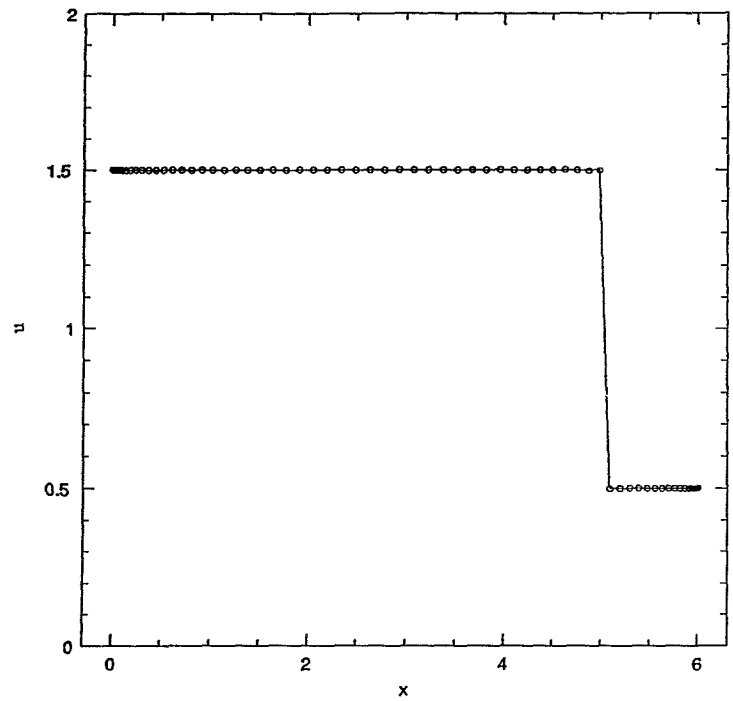

FIG. 6.2. *Linear advection of a discontinuous solution, $N = 64$, $K = 1$ at time $t = 2.0$.*

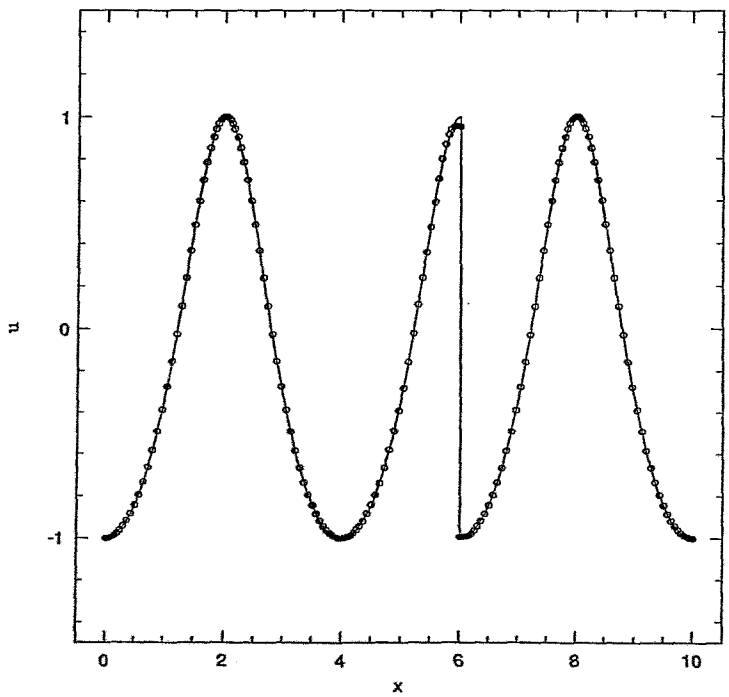

FIG. 6.3. *Linear advection of a discontinuous solution, $N = 40$, $K = 5$ at time $t = 1.0$.*

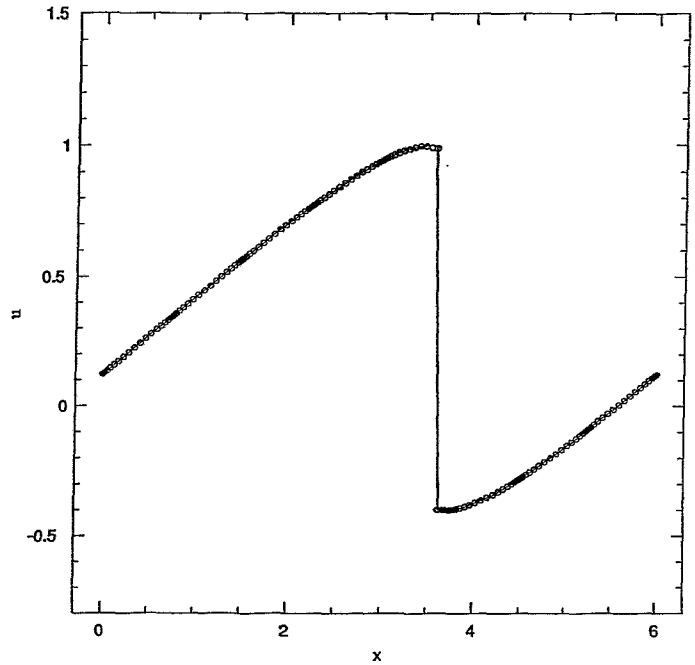

FIG. 6.4. *Solution to inviscid Burgers equation for* $N = 20$, $K = 8$ *at time* $t = 2.0$.

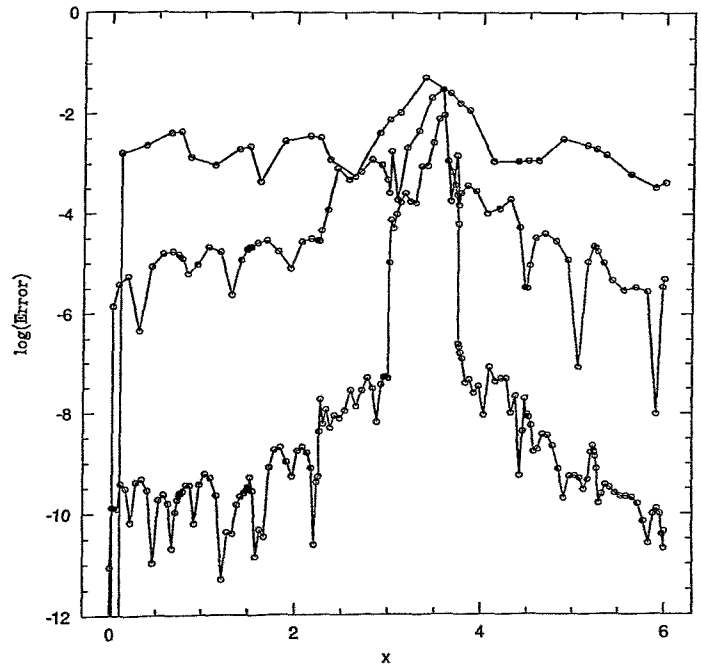

FIG. 6.5. *Errors in the solution of the inviscid Burgers equation for* $N = 5, 10, 20$, *and* $K = 8$ *at time* $t = 2.0$.

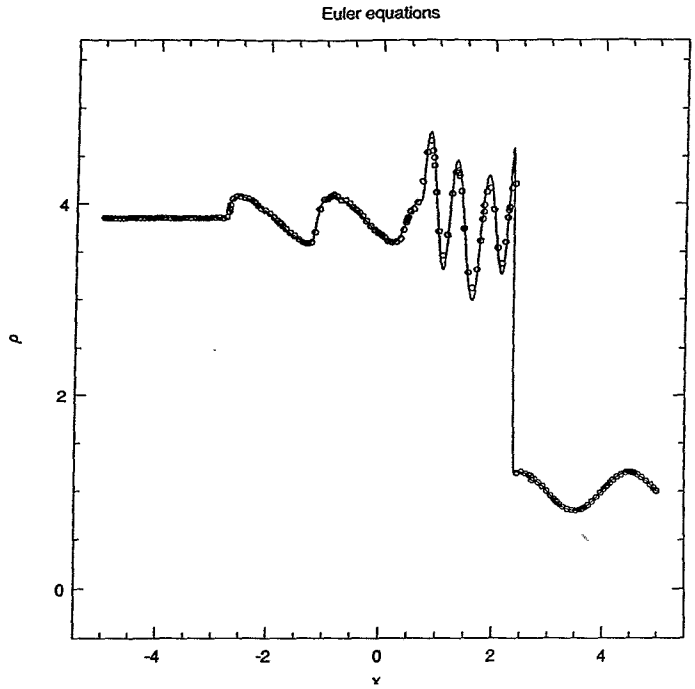

FIG. 6.6. *(a) Interactions between a shock wave and density waves with $N = 10$, $K = 22$ (201 grid points) at time $t = 1.8$. The solid represents the solution obtained by the third order ENO finite difference method with 1200 grid points (courtesy of Wai-Sun Don and David Gottlieb, Brown University).*

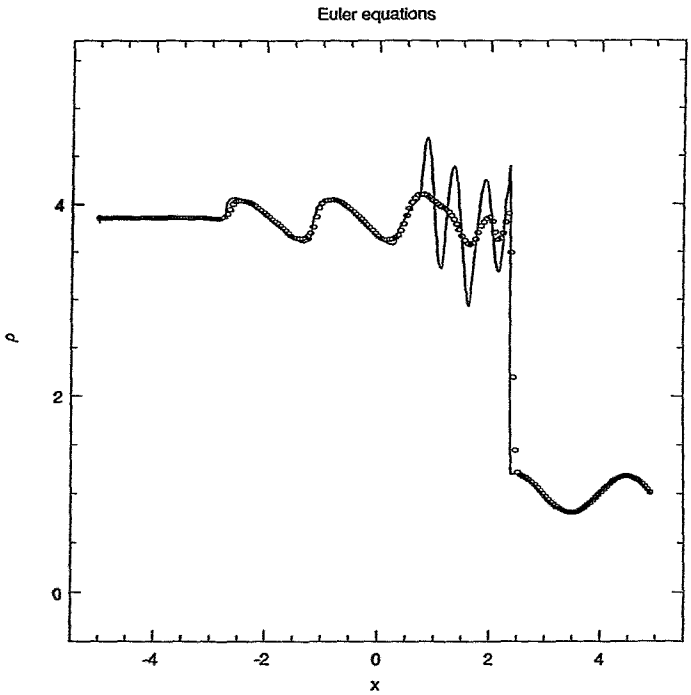

FIG. 6.6. *(b) The same problem as in the previous figure. Result obtained by a second order MUSCL scheme using 200 grid points (courtesy of Wei Cai and Chi-Wang Shu).*

REFERENCES

[1] W. CAI, D. GOTTLIEB, AND A. HARTEN, *Cell averaging Chebyshev methods for hyperbolic problems*, Report No. 90-72, ICASE, 1990.

[2] W. CAI, D. GOTTLIEB, AND C. SHU, *Non-oscillatory spectral Fourier methods for shock wave calculations*, Math. Comp., 52 (1989), pp. 389–410.

[3] W. CAI AND C. SHU, *Uniform high order spectral methods for one and two dimensional Euler equations*. Submitted for publication.

[4] C. W. GEAR, *Numerical Initial Value Problems in Ordinary Differential Equations*, Prentice-Hall, 1973.

[5] D. GOTTLIEB AND S. A. ORSZAG, *Numerical Analysis of Spectral Methods: Theory and Applications*, SIAM, Philadelphia, 1977.

[6] G. E. KARNIADAKIS, *Spectral element simulations of laminar and turbulent flows in complex geometries*, Appl. Num. Math., 6 (1989), p. 85.

[7] G. E. KARNIADAKIS, E. T. BULLISTER, AND A. T. PATERA, *A spectral element method for solution of two- and three-dimensional time dependent Navier-Stokes equations*, in Finite Element Methods for Nonlinear Problems, Springer-Verlag, 1985, p. 803.

[8] Y. MADAY AND A. T. PATERA, *Spectral element methods for the Navier-Stokes equations.*, ASME, State-of-the-art surveys in Computational Mechanics, (1987).

[9] A. T. PATERA, *A spectral element method for Fluid Dynamics; Laminar flow in a channel expansion*, J. Comput. Phys., 54 (1984), p. 468.

[10] P. L. ROE, *Approximate Riemann solvers, parameter vectors, and difference schemes*, J. Comput. Phys., 43 (1981), pp. 357–372.

[11] E. M. RØNQUIST, *Optimal spectral element methods for the unsteady three-dimensional incompressible Navier-Stokes equations*, PhD thesis, Massachusetts Institute of Technology, 1988.

[12] D. SIDILKOVER, *High order shock locating methods.* Submitted for publication.

[13] P. K. SWEBY, *High resolution schemes using flux limiters for hyperbolic conservation laws*, SIAM J. Numer. Anal., 21 (1984), pp. 995–1011.

[14] H. VANDEVEN, *Family of spectral filters for discontinuous problems*, PhD thesis, CMAP - Ecole Polytechnique, France, 1989.